Crystal Structure of the K12M/G15A Triosephosphate Isomerase Double Mutant and Electrostatic Analysis of the Active Site†

Diane Joseph-McCarthy,‡,§ Elias Lolis,‡,‖ Elizabeth A. Komives,⊥,# and Gregory A. Petsko*,△

Departments of Biochemistry and Chemistry, Rosenstiel Basic Medical Sciences Research Center, Brandeis University, Waltham, Massachusetts 02254-9110, Departments of Chemistry and Biochemistry, Harvard University, Cambridge, Massachusetts 02138, and Department of Chemistry, Massachusetts Institute of Technology, Cambridge, Massachusetts 02139

Received August 5, 1993; Revised Manuscript Received October 28, 1993⊗

ABSTRACT: The crystal structure of the yeast triosephosphate isomerase (TIM) double mutant K12M/G15A has been solved to 2 Å by X-ray diffraction, and the effects of changing the positively charged lysine to the neutral methionine have been analyzed. The mutant enzyme was crystallized in the presence of the tight-binding inhibitor phosphoglycolohydroxamate, under standard conditions for obtaining crystals of the enzyme–inhibitor complex. The crystals obtained were of the same crystal form as the *un*liganded wild-type enzyme. The three-dimensional structure confirms that the Lys-12 to Met mutation prevents the enzyme from binding substrate and reveals that the reason is electrostatic and not steric. The substrate-binding loop is in its open position and the Met side chain points away from the active site. Overall, the mutant structure is very similar to that of the wild-type unliganded enzyme. The electrostatic potential at the active site of the mutant enzyme is, however, very different from that of the wild type. It has been postulated previously that Lys-12 may play a role in stabilizing the negative charge in the transition state. This K12M/G15A structure suggests that the active-site Lys, which is strictly conserved, is required for TIM to be able to bind its dianionic substrate.

Triosephosphate isomerase (TIM; EC 5.3.1.1), the central enzyme in the glycolytic pathway, catalyzes the interconversion of the two products of the aldolase reaction, D-glyceraldehyde 3-phosphate (D-GAP) and dihydroxyacetone phosphate (DHAP). Since only D-GAP is able to proceed down the pathway, TIM insures a net positive yield of ATP from the oxidation of glucose to pyruvate. Triosephosphate isomerase is ubiquitous, and its sequence is about 50% conserved from bacteria to humans. The enzyme from all sources is a homodimer of overall molecular weight 56 000.

TIM is a very efficient catalyst: k_{cat}/K_m in the direction D-GAP as substrate is in excess of 10^8 M^{-1} s^{-1}, which is comparable to the diffusion-controlled association rate of small molecules with proteins (Albery & Knowles, 1976). Studies of the viscosity dependence of the enzyme-catalyzed reaction have shown that the TIM reaction is indeed diffusion-controlled (Blacklow et al., 1988) and is under no further evolutionary pressure to increase the rate of any of the chemical steps of catalysis (Knowles & Albery, 1977).

Because of the apparent simplicity of the isomerization reaction that it catalyzes, TIM has been the subject of many studies by a wide variety of biochemical and biophysical techniques. High-resolution crystal structures are available for the chicken muscle (Banner et al., 1975), yeast (Lolis et al., 1990), and trypanosomal (Wierenga et al., 1987) enzymes, and a number of enzyme–substrate and enzyme–inhibitor complexes have also been analyzed at various resolutions (Phillips et al., 1977; Alber et al., 1981; Wierenga et al., 1991b). TIM is the prototype of a family of over 30 enzymes that share a common folding motif consisting of an eight-stranded parallel β-barrel with connecting α-helices (Farber & Petsko, 1990) (Figure 1). The active sites of all members of this family are at the carboxy-terminal end of the β-sheet. The catalytic residues usually come from loops that connect the β-strands to the helices.

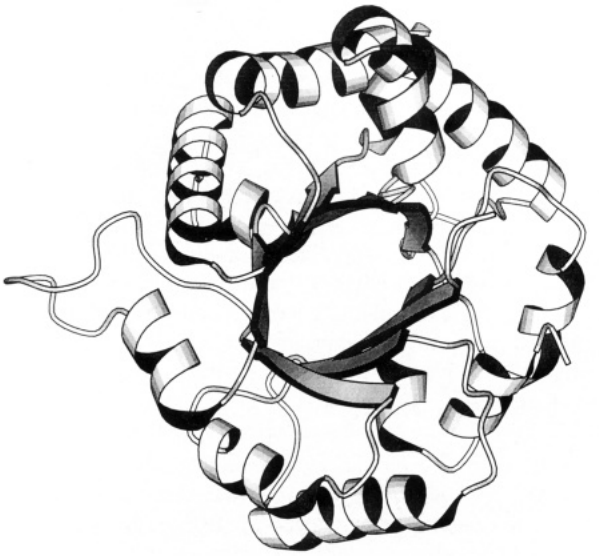

FIGURE 1: Ribbon diagram of the polypeptide chain fold of the monomer of triosephosphate isomerase, drawn using the program MOLSCRIPT (Kraulis, 1991). The view is directly into the active site, which is a pocket at the C-terminal end of the parallel β-barrel in the center of the picture.

† Supported in part by USPHS Grant GM 26788 to G.A.P. Also, D.J. thanks the American Association of University Women for a dissertation fellowship.

‡ Massachusetts Institute of Technology.

§ Present address: Department of Biological Chemistry and Molecular Pharmacology, Harvard Medical School, Boston, MA 02115.

‖ Present address: Department of Pharmacology, Yale University School of Medicine, 333 Cedar Street, New Haven, CT 06510.

⊥ Harvard University.

Present address: Department of Chemistry, University of California at San Diego, La Jolla, CA 92093.

△ Brandeis University.

⊗ Abstract published in *Advance ACS Abstracts,* February 1, 1994.

0006-2960/94/0433-2815$04.50/0

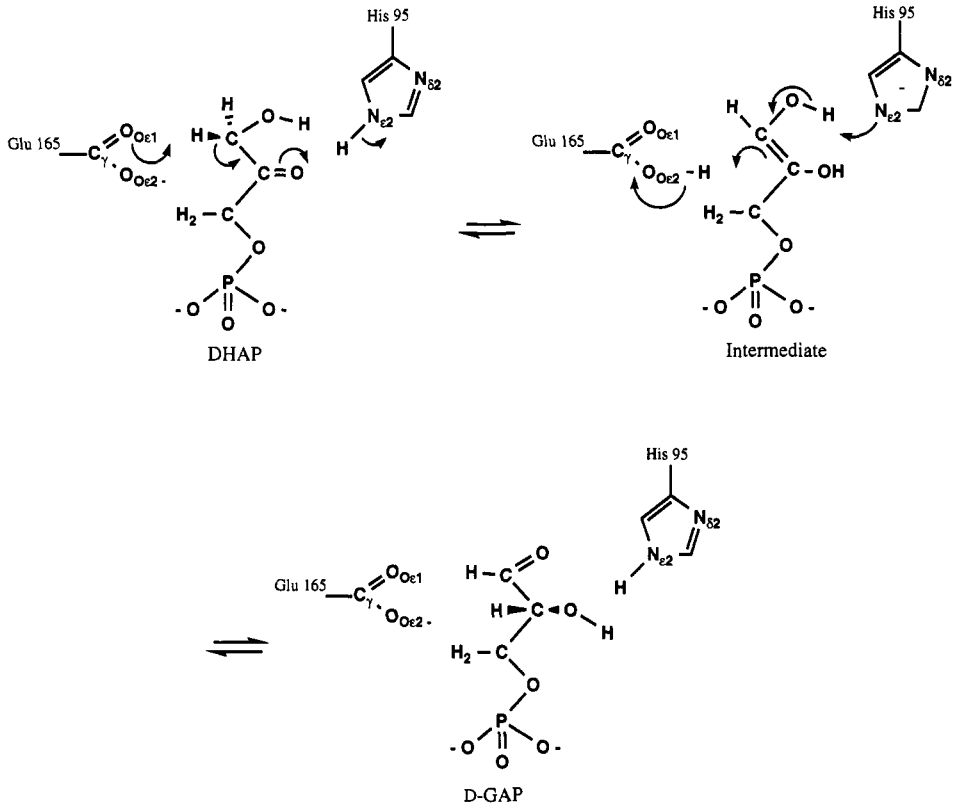

FIGURE 2: Mechanism of the triosephosphate isomerase reaction. The active-site residues have been assigned roles on the basis of X-ray structural studies of enzyme–inhibitor complexes [e.g., Davenport et al. (1991)] and site-directed mutagenesis [summarized in Knowles (1991)].

The current hypothesis for the catalytic mechanism of TIM involves acid–base chemistry in which the side-chain carboxylate of Glu-165 abstracts a proton from the substrate carbon atom (Joseph-McCarthy et al., 1994), while the imidazole ring of His-95 in its neutral form protonates the substrate carbonyl group (Alber et al., 1981, 1987; Knowles, 1991) (Figure 2). Site-directed mutagenesis of these residues has confirmed the general features of this mechanism (Raines et al., 1986; Nickbarg et al., 1988; Komives et al., 1991). A combined quantum mechanics/molecular dynamics simulation of the TIM reaction has suggested a number of other residues, including Lys-12,[1] as participants in catalysis by electrostatic stabilization of the transition state (Bash et al., 1991).

In the structure of the complex of yeast triosephosphate isomerase with phosphoglycolohydroxamate (PGH; Collins, 1974), the side-chain Nε of Lys-12 hydrogen bonds to the C2 oxygen of the substrate and also forms a salt bridge with the side-chain carboxylate of Glu-97 (Davenport et al., 1991) (Figure 2). Lys-12 is strictly conserved in all 13 known sequences of TIM from organisms ranging from *Escherichia coli* to humans (Lolis et al., 1990). It has been postulated (Alber et al., 1987; Bash et al., 1991; Knowles, 1991) that the positive charge of the Lys-12 side chain is one of the structural features of the active site responsible for the electrostatic stabilization of the enediolate-like transition state for proton transfer. To test this hypothesis, Lys-12 has been mutated to Met in the yeast enzyme [Lodi et al. (1994), preceding article in this issue]. Fourier transform infrared studies and direct binding experiments have shown that the K12M mutant of yeast TIM does not bind substrate; k_{cat} for the preparation of the mutant has been measured as 0.018 s^{-1} and attributed to contaminating wild-type enzyme (Lodi et al., 1994).

[1] This is the yeast TIM numbering; it is Lys-13 in the chicken muscle enzyme.

In the first experiments that generated the K12M mutant, a second change—G15A—was also made. Subsequent analysis of the single K12M mutant enzyme showed that the additional G15A mutation had no discernible effect on the properties of the enzyme. Residue 15 is not part of the active site and is not involved in the reaction, and we expect that the structure of the K12M/G15A double mutant will be essentially identical to that of the single K12M mutant. In this article, we report the high-resolution crystal structure of the double mutant and present an electrostatic analysis of the altered active site. We conclude that one function of the conserved Lys-12 in TIM is to generate a net positive charge at the active site, so that anionic substrates will bind.

MATERIALS AND METHODS

Reagents. Glucuronolactone, histidine, streptomycin, ampicillin, reduced nicotinamide adenine dinucleotide, and QAE Sephadex A-120 were obtained from Sigma Chemical Co. (St. Louis, MO). Poly(ethylene glycol) 4000 was obtained from U.S. Biochemicals (Cleveland, OH). PGH was prepared by J. Belasco. All other reagents were from commercial sources and were used without further purification.

Proteins. The gene for wild-type TIM from yeast was subcloned into a derivative of pBS+/− that has been described (Blacklow & Knowles, 1990). This phagemid vector allowed the efficient production of single-stranded DNA for mutagenesis. The phagemide contains, on an *Eco*RI–*Pst*I fragment, the *trc* promoter upstream from the complete gene for yeast TIM. The mutant in which lysine-12 was changed to methionine was constructed by using the oligonucleotide-directed mutagenesis kit available from Amersham (Arlington Hts., IL), which follows the method of Nakamaye and Eckstein (1986). The sequence of the primer used in the mutagenesis reaction was 5′-GGA AGC GTT TAA CAT AAA GTT ACC ACC-3′, which hybridizes to the coding strand of the yeast

TIM gene and encodes for the sequence, 5′-GGT GGT AAC TTT ATG TTA AAC GCT TCC-3′, which encodes for the protein sequence, GGNFMLNAS. This oligo changed the lysine at position 12 to methionine, but also inadvertently changed the glycine at position 15 to alanine. The sequence of the entire gene was determined to ensure that no other inadvertent mutations were created during mutagenesis. The gene for the mutant protein was subsequently subcloned into the high-expression vector pKK223-3 (Pharmacia LKB, Piscataway, NJ), using the unique *Eco*RI and *Pst*I sites to avoid instability of the phagemid upon large-scale growth. The resulting plasmids contain tandem promoters (*tac* from pKK223-3 and *trc* from the *Eco*RI–*Pst*I phagemid fragment), which allowed the production of 50–80 mg of protein/L of cells. The expression vectors were used to transform *Escherichia coli* strain DF502, which is a *strep*^{R}, *tpi*$^-$ strain that was kindly provided by D. Fraenkel and has been previously described (Straus & Gilbert, 1985).

Large amounts of pure protein were prepared by growing the bacterial transformants in a final volume of 10 L of M63 salts (Miller, 1972) containing casamino acids (0.5% w/v), glucuronolactone (0.4% w/v), glycerol (0.1% w/v), $MgSO_4$ (1 mM), thiamine (1 mg/mL), L-histidine (80 mg/L), streptomycin (100 mg/L), and ampicillin (200 mg/L). Cells were harvested after 12–20 h by centrifugation at 3000*g*. The cells were lysed in a continuous flow French pressure cell (Aminco, Urbana, IL), and the lysate was centrifuged at 8500*g* for 1 h to remove cell debris. The ammonium sulfate fraction from 55% to 90% saturation was collected and dialyzed against TE buffer (10 mM Tris-HCl (pH 7.8) and 1 mM EDTA) overnight. The following day, the crude protein was loaded onto a 300-L column of QAE Sephadex A-120 equilibrated with TE buffer and eluted with a linear gradient of 0–300 mM KCl (1 L to 1 L). The proteins were finally purified on a MonoQ 10/10 column using the same gradient. The purity of the proteins was assessed by silver staining overloaded 15% SDS–PAGE gels (Laemmli, 1970). Concentration of the proteins was afforded by Centriprep and Centricon concentration (Amicon, Danvers, MA). The double mutant TIM, K12M/G15A, was dialyzed against 200 mM Tris-HCl (pH 6.8), 1 mM EDTA, and 1 mM β-mercaptoethanol by four changes of buffer in Centricon concentrators.

Crystallization and X-ray Diffraction Data Collection. Although the K12M and K12M/G15A mutants of yeast TIM were essentially devoid of catalytic activity, their affinities for inhibitors such as phosphoglycolohydroxamate were unknown. Therefore, we followed our normal practice and crystallized the K12M/G15A mutant in the presence of a high concentration of PGH under conditions established for the wild-type enzyme–PGH complex. Protein crystals were grown by precipitation from poly(ethylene glycol) 4000 at room temperature in 100-μL portions containing TIM (20 mg/mL, 0.8 mM in active site) and PGH (1.5 mM final concentration) in one-half dram vials loosely fitted with cork stoppers. The mutant crystallized readily in flattened prisms with a symmetry of space group $P2_1$ and unit cell dimensions a = 61.2 Å, b = 97.7 Å, c = 48.8 Å, and β = 90.4°. There is one complete dimeric molecule in the crystallographic asymmetric unit. This result was surprising: the mutant in the presence of PGH has essentially the same crystal form as the native wild-type enzyme in the absence of PGH (Lolis et al., 1990).

X-ray diffraction data were collected to 1.9-Å resolution on a Siemens multiwire area detector with copper Kα X-rays from an Elliot GX13 rotating anode generator. The crystal was maintained at a temperature of 4 °C by a stream of cold dry air. Data were collected as a series of 0.2-deg oscillation frames and were reduced using the program XDS (Kabsch, 1988). The merging R factor for symmetry-related reflections was 3.4% for the 41 538 reflections with background-corrected intensity greater than zero.

The data collected from 1.94- to 16.67-Å resolution were 70% complete with 30 028 reflections measured of the 42 702 possible reflections. However, the shell of data measured from 1.94- to 2.04-Å resolution was only 24% complete, and therefore the data set was truncated to 2-Å resolution. The overall completeness of the data set from 2- to 16.67-Å resolution was 76% and included 29 383 of the possible 38 724 reflections. The missing data were distributed throughout reciprocal space. For the shell of data from 2.2- to 2.0-Å resolution, the average I/σ was 3.3.

Model Building and Structure Refinement. To avoid bias, the initial electron density map calculated was an "annealed omit map" in which the phases were derived from simulated annealing refinement (Brünger et al., 1987) using the native yeast TIM X-ray structure (Lolis et al., 1990) with Lys-12 "mutated" to Ala as the initial model. Standard X-PLOR protocols were followed for determination of the ideal weight to be used for the diffraction energy terms, conventional positional refinement, slow-cooling simulated annealing, grouped, unrestrained B factor refinement, and restrained, individual B factor refinement. Standard parameters for the empirical potential energy function were used for all X-PLOR runs. The initial model with Lys-12 omitted was subjected to X-PLOR positional refinement, followed by slow cooling from 3000 to 300 K and a final round of positional refinement. All data from 16- to 2-Å resolution (29 306 reflections) were included in the refinement. The overall R factor dropped from an initial value of 0.424 to 0.264. A $3F_o - 2F_c$ electron density map was calculated to examine the active site, which showed clear density for the methionine side chain at position 12 in both subunits and also for the β-carbon of the alanine that had been accidentally introduced at position 15. Before we attempted model the changes in the active site, the entire structure was inspected manually and changes were made to other parts of both subunits to improve the fit of surface side chains to the electron density. The rebuilt structure was subjected to another round of X-PLOR positional, slow cooling, and positional refinement. During this run, the R factor dropped from a starting value of 0.336 to 0.262. Grouped, unrestrained and then individual, restrained B factor refinement further reduced the R factor to 0.242. Again, a $3F_o - 2F_c$ electron density map was calculated and the entire structure was examined. At this point, residue 12 was mutated on the computer from Ala to Met to match the clear side-chain electron density, residue 15 was changed from Gly to Ala in each subunit, and these side chains were fitted into their electron density.

Crystallographic waters were added to the structure by using the WATERHUNTER suite of programs (S. Sugio, R. C. Davenport, and G. A. Petsko, unpublished results), consisting of the programs Waterhunter, Watershufle, and Watermerge. The program Waterhunter searches an input $F_o - F_c$ difference Fourier map for peaks (>3.5σ density) and places water molecules in those peaks that do not overlap with the input structure. Only those waters that are more than a specified cutoff away from neighboring atoms (2.2 Å) and that can make reasonable hydrogen bonds as specified by a minimum and maximum allowed hydrogen-bond distance (2.2–4.5 Å) are placed. The program Watershufle shuffles the water coordinates so that they correctly overlap in space with the region around the protein coordinates. The program Wa-

FIGURE 3: Electron density for the active site of the K12M/G15A double mutant of yeast triosephosphate isomerase, in stereo. Residues Met-12, His-95, Ser-96, Glu-97, Glu-165, and Thr-75B (from the other subunit in the homodimer) are shown in thick black lines in a $2F_o - F_c$ electron density map contoured at 1.5σ.

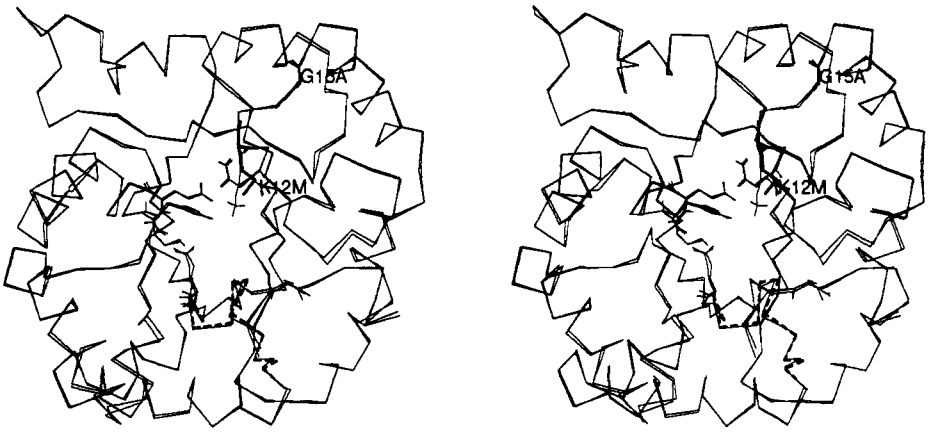

FIGURE 4: Superposition of the K12M/G15A mutant and the unliganded wild-type structure of subunit one by least-squares optimization of all backbone atoms, shown in stereo (cross-eyed). All atoms are shown for Met-12 and Gly-15 in thick black lines, and Asn-10, His-95, Ser-96, Glu-97, and Glu-165 are in thin black lines. Only α-carbons are drawn for the rest of subunit one; the loop α-carbons are indicated by dashed lines.

termerge deletes waters that are too close to other waters (2.4 Å apart) or that have high *B* factors (>50.0) and then merges the resulting water coordinate file with the coordinate file originally input.

The positions of the 176 waters added by the WATERHUNTER programs to the K12M/G15A structure were checked manually by again examining the structure and the $3F_o - 2F_c$ electron density map on the graphics system; 40 of the waters were deleted and 5 additional waters were added. The structure of the dimer with 141 crystallographic waters was subjected to X-PLOR positional, slow-cooling (this time only from 2000 to 300 K) simulated annealing, positional, grouped *B* factor, and individual *B* factor refinement. Only the data from 6 to 2 Å (28 004 reflections) were used in this and all subsequent refinement runs. The *R* factor dropped from 0.366 to 0.196. The WATERHUNTER programs were run again, adding 96 new waters. This structure was rebuilt on the graphics system using a $3F_o - 2F_c$ electron density map that was calculated before the new waters were added; 42 waters were deleted and 15 added by hand. The resulting structure with 210 crystal waters were subjected to a final round of X-PLOR positional, grouped *B* factor, and individual *B* factor refinement. The *R* factor dropped from 0.370 to a final value of 0.197 vs all data.

Electrostatic Potential Calculations. Electrostatic maps of the surfaces of the K12M/G15A mutant dimer and of the native yeast TIM dimer, with and without crystallographic waters, were calculated. The program UHBD (University of Houston Brownian Dynamics) (Davis et al., 1991) was used for the calculation with an interior dielectric constant of 2.0, a solvent dielectric constant of 80.0, a temperature of 300 K, and an ionic strength of 0.0. UHBD uses a finite difference approach for solving the linearized Poisson–Boltzmann equation. This is a large problem for our case: the size of the TIM dimer is approximately $75 \times 45 \times 35$ Å^3. The electrostatic maps were calculated with a $100 \times 100 \times 100$ grid and a grid spacing of 1.5 Å. At the grid boundary, the potential due to the molecule is set to the value of the potential of a single Debye–Huckel sphere with the net charge of the dimeric molecule (–6.0 for the mutant structure and –4.0 for the native wild-type structure) and a radius of 35.0 Å. The resulting electrostatic potential maps were examined using the program Quanta on an IRIS workstation.

RESULTS

At 2-Å resolution, the final *R* factor for the structure including 210 crystallographic water molecules is 0.197, and at 2.5-Å resolution the *R* factor is 0.183. The geometry of the structure is quite good. The overall root-mean-square (rms) deviation of bond lengths from ideality is 0.020 Å, which is within experimental error; the rms deviation of bond angles is 3.4°. Only 48 bonds differ from ideality by more than 0.06 Å, and only nine differ by more than 0.1 Å. The largest difference is 0.144 Å for a Cβ–Cγ2 bond. Only 69 angles deviate from ideality by more than 10°, and the largest deviation is 21.2°. There are no dihedral angles that deviate from ideality by more than 90° and no improper dihedral angles that deviate by more than 20°. When all of the distances

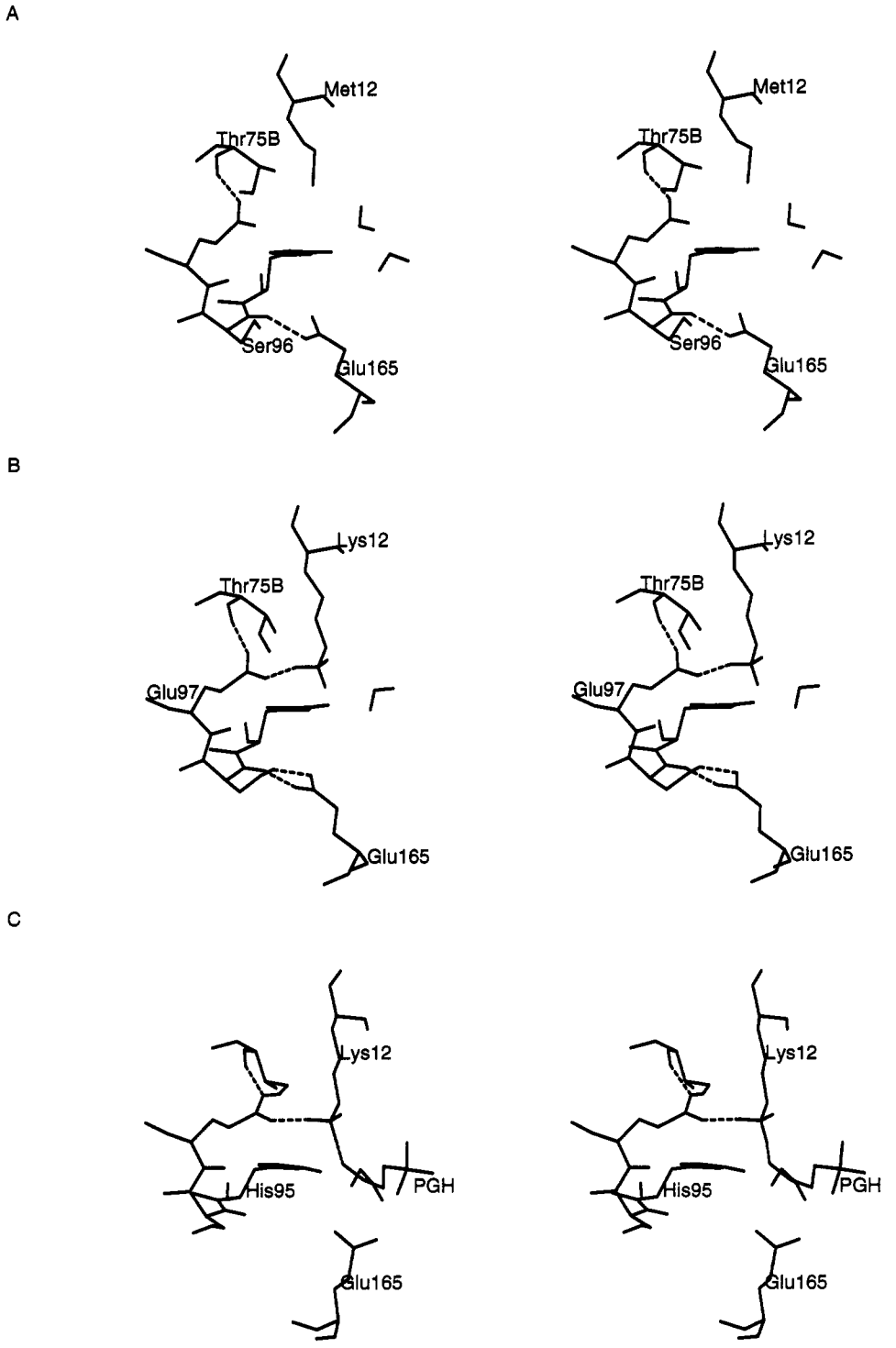

FIGURE 5: Stereoviews of residues Lys/Met-12, His-95, Ser-96, Glu-97, Thr-75B, Glu-165, and active-site bound waters/PGH for (A) the K12M/G15A mutant structure, (B) the unliganded wild-type structure, and (C) the liganded (PGH) wild-type structure. Hydrogen bonds are drawn as dashed lines.

between non-hydrogen atoms that are less than 4.0 Å are examined, most of them are hydrogen bonds. Only 18 of these distances are less than 3.0 Å, and the smallest such distance is 2.6 Å.

One of the major features of the active site of the K12M/G15A mutant is that, although there is ample room in the active site to accommodate the substrate analog PGH, no density corresponding to either the inhibitor or to a bound sulfate or phosphate group is observed. All other crystal forms of TIM have either an inhibitor or an anion bound in the active site (Wierenga et al., 1991a). In the K12M structure, however, there are two water molecules bound in the active site. Further, the substrate-binding flexible loop (residues 166–176) is in the open conformation. This loop makes no hydrogen bonds to protein, except for Tyr-164 to Trp-168, and it projects out into solvent as in the unliganded wild-type structure (Joseph et al., 1990). Subunit one active-site residues are shown in a $2F_o - F_c$ electron density map in Figure 3. The subunit two active site, which is not shown, is very similar, except that the side chain of Met-12 is best fit to its electron density with the Sδ atom slightly closer to Glu-97 than the Cε atom. (In subunit one, the side-chain conformation of Met-12 is such that Sδ is farther away from Glu-97 than Cε.)

When the K12M/G15A mutant structure is superimposed onto the yeast TIM–PGH complex structure, it is clear that the structures are very similar except for the flexible loop.

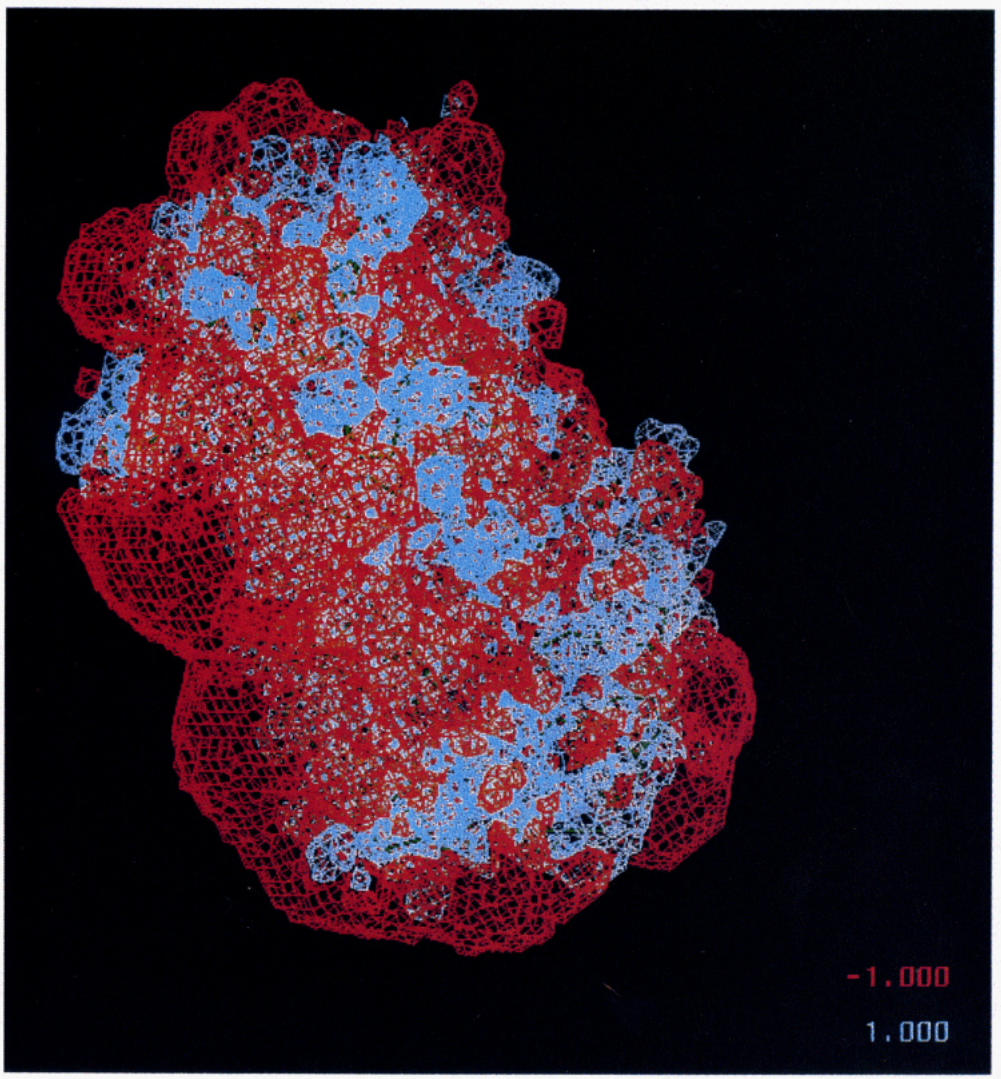
-1.000
1.000

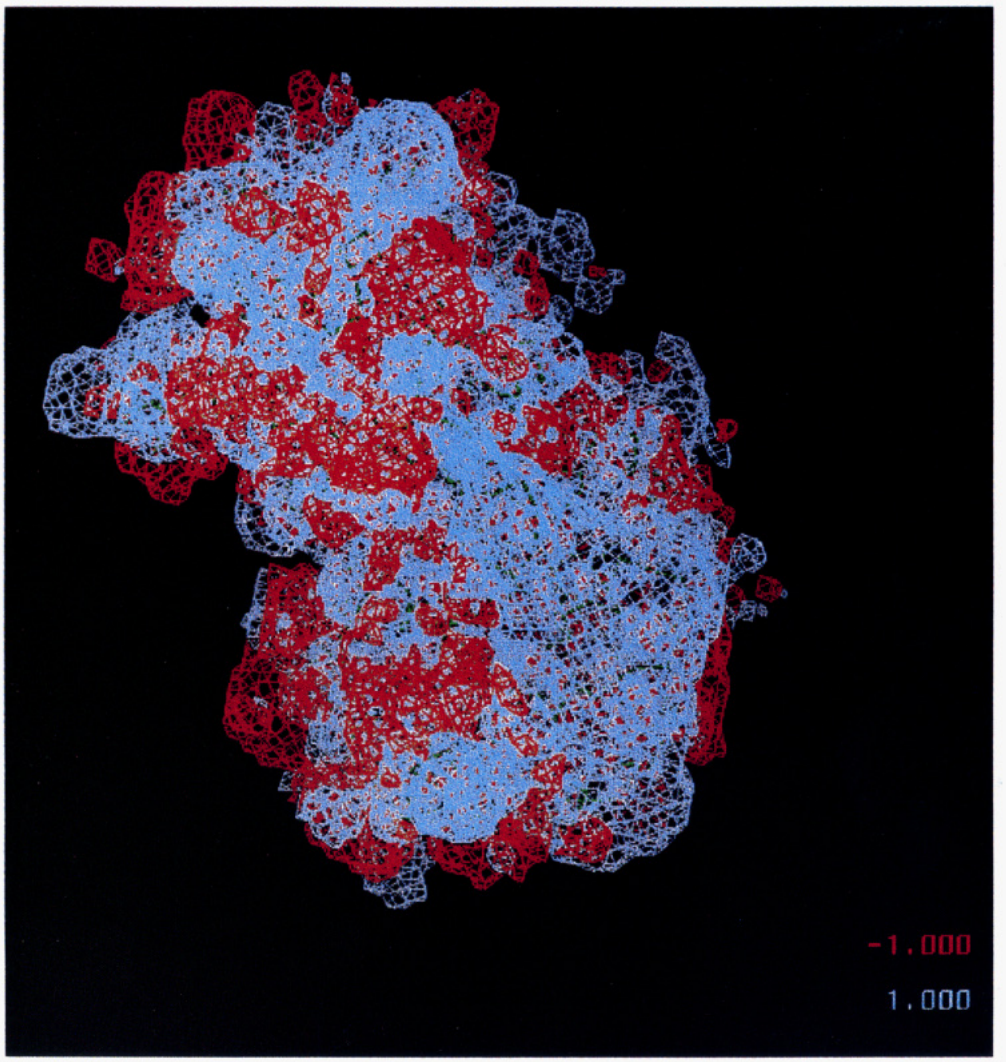

FIGURE 6: Electrostatic potential maps of the K12M/G15A mutant structure and the unliganded wild-type structure. (A, top left) The K12M/G15A dimer in the same orientation as the electrostatic maps in B (bottom left) and C (right). Met-12 and the loop residues of subunit one are shown in thick black lines. Electrostatic maps of the mutant structure (B) and the unliganded wild-type structure (C) are shown contoured at ±1.0 kcal/mol values of the electrostatic potential. The +1.0 kcal/mol contour level is in blue, and the −1.0 kcal/mol contour level is in red.

Matching backbone atoms of residues 2–161 and 181–248, the rms difference for these atoms between the two structures is 0.50 Å. The two bound waters in the active site of the mutant are located where the sugar moiety of the substrate (specifically atoms C1 to C2) is expected to bind. One of the waters is 1.06 Å from the oxygen atom that is bonded to the nitrogen atom of PGH, and the other is 1.27 Å from the carbon atom that is bonded to the phosphate bridging oxygen of PGH. The oxygen atoms of the two bound water molecules are 2.7 Å apart, and one of these oxygens is 3.0 Å away from the Nϵ2 of His-95. (These numbers are for active-site residues of subunit one. Throughout this article, only the subunit one values are discussed whenever the subunit two values are very similar.)

When the K12M/G15A mutant structure is superposed on the unliganded wild-type structure, the rms difference is 1.05 Å for all atoms and 0.43 Å for backbone atoms. When the two structures are superimposed by matching all backbone atoms, examination of the subunit one active-site residues (specifically, residues 9–13, 94–98, 125–130, 162–180, and 210–212) reveals that only the Glu-129, Ile-170, Asp-180, and Ser-211 side chains are in significantly different conformations. The Glu-129 Oϵ1 differ by 2.59 Å (Oϵ2 by only 0.53 Å), Ile-170 Cγ1 by 1.82 Å, Asp-180 Oδ2 by 1.73 Å (Oδ1 by 1.28 Å), and Ser-211 Oγ by 2.45 Å. (The differences for the side-chain atoms directly preceding each of these are all fairly small, e.g., Glu-129 Cδ differ by 0.57 Å.) The substrate-binding loop (residues 166–176) in the mutant structure is in essentially the same open conformation as in the unliganded wild-type structure (Joseph et al., 1990). The two most obvious differences for the loop residues are Ile-170 Cγ1 (1.82 Å) and Thr-172 Oγ1 (only 0.68 Å). Figure 4 shows a stereoview of the subunit one α-carbons of both structures, with all atoms for several important active-site residues drawn and Met-12, Ala-15, and the loop residues shown in heavy lines.

The hydrogen-bonding patterns of several key active-site residues (Lys/Met-12, His-95, Ser-96, Glu-97, Glu-165, Thr-75B, and active-site waters/PGH) for the K12M/G15A mutant structure, the native wild-type structure, and the PGH complex wild-type structure are shown in Figure 5. In all three structures the side chain of Glu-97 is hydrogen-bonded to the amide nitrogen of Thr-75B (part of the interdigitating loop from the other subunit). In both the unliganded and complexed wild-type structures, Glu-97 and Lys-12 form a salt bridge. In the unliganded wild-type structure, Ser-96 Oγ hydrogen bonds to Glu-165 Oϵ1, whereas in the mutant structure Ser-96 Oγ forms a weak hydrogen bond to the amide nitrogen of Glu-97 instead. (The side chain of Glu-165 does hydrogen bond to the amide nitrogen of Ser-96 in both the mutant and the unliganded wild-type structures.) The side chain of Met-12 in the mutant structure is not involved in any obvious polar interactions.

The conformation of the side chain of Met-12 in the mutant structure closely follows that of Lys-12 in the unliganded wild-type structure up to Cγ, and then the side chains diverge with the Sδ and Cε of the Met side chain moved somewhat away from Glu-97 and toward Gly 232. The distances (for subunit one) between corresponding atoms of the Lys-12 and Met-12 side chains (superimposing all backbone atoms) are 0.11 Å for Cα, 0.24 Å for Cβ, 0.36 Å for Cγ, 1.55 for Cδ–Sδ, and 0.88 Å for Cε. The Met-12 conformation in subunit two is similar, except that Sδ is somewhat closer to Cδ of Lys-12 (they are 0.80 Å apart) and Cε is rotated even farther away from the Glu-97 side of the active site (the Cε atoms are 3.33 Å apart) than in subunit one. Lys-12 is in virtually the same conformation in the liganded wild-type structure as in the unliganded wild-type structure, and therefore the comparison of the position of Met-12 with that of Lys-12 in the liganded structure is very similar to the comparison with the position of Lys-12 in the unliganded structure. Met-12 is pushed to the side of the binding pocket relative to Lys-12 in the wild-type structures, and there is thus ample room in the active site for substrate.

The electrostatic map of the K12M/G15A mutant with crystallographic waters has a minimum value of −120.4 kcal/mol and a maximum value of 97.6 kcal/mol, where the units of energy are per unit of charge. Similarly, the map of the wild-type structure with crystallographic waters has a minimum of −116.8 kcal/mol and a maximum of 103.4 kcal/mol. Both electrostatic maps were examined at various contours of constant potential, including −1.0 and 1.0 kcal/mol, −0.5 and 0.5 kcal/mol, and −0.2 and 0.2 kcal/mol. The sign of the contour is determined by the signs of the charges on the protein, and the absolute value of the contour level decreases as the distance from the protein increases. A single positive test charge at a position on the −1.0 kcal/mol contour would have a favorable energy of −1.0 kcal/mol. Figure 6 shows the orientation of the structures, the electrostatic map for the mutant, and the map for the unliganded wild-type structure at both the −1.0 and 1.0 kcal/mol contours. The structures are oriented so that the viewer is looking directly into the mouth of the subunit one active site, and the entire electrostatic map is displayed. The maps at the −1.0 and 1.0 contour levels show that the active-site pocket is negative for the mutant and amphipathic, although primarily positive, for the native structure. At these contour levels, the maps extend approximately 5 Å from the edge of the molecule. At the −0.2 and 0.2 kcal/mol contours (which extend farther away from the molecule), there is an even more dramatic difference between the two structures. The surface of the mutant structure is almost entirely negative, whereas the surface of the native wild-type structure is entirely positive. At the ±0.2 kcal/mol contour levels, however, the maps extend 10–20 Å from the edge of the molecule, which may be pushing the limit of the calculation. Although the mutant and wild-type structures have 210 and 139 crystallographic waters, respectively, the calculations excluding the crystallographic waters yielded essentially the same results at the ±1.0 and ±0.2 kcal/mol contours.

DISCUSSION

We have confirmed by structural studies that the inhibitor PGH does not bind to the K12M/G15A mutant isomerase and that the substrate-binding loop is in the open conformation in this mutant. We have also shown that Met-12 does not sterically prevent the substrate from binding. The loss of activity of the K12M mutant of yeast TIM must therefore be due to another cause. Since Lys-12 presumably bears a positive charge in the native structure, we have examined the electrostatic potential distribution of both the mutant and wild-type enzymes. We find that in the K12M mutant enzyme the active-site surface has an overall negative charge, in contrast to the open wild-type enzyme that has a positively charged active-site region where the phosphate of the substrate binds.

Several other mutants have been made to elucidate the role that Lys-12 and the substrate-binding loop play in stabilizing the enzyme intermediate and/or in orienting the substrate. Lys-12 has also been changed to Arg and His (Lodi et al., 1994), Thr-172 (the center of the loop) has been changed to Asp (E. Lolis and M. Kanaoka, unpublished results), and a TIM mutant lacking four central loop residues (170–173) has been studied (Pompliano et al., 1990). All of these mutants are in yeast TIM, except for the loop deletion mutant, which is in chicken TIM. Alone among them all, the K12M mutant does not bind substrate. Semiempirical quantum mechanical calculations to investigate the extent to which various residues stabilize the enediol(ate) intermediate have shown that, although Lys-12 is most important in lowering the barrier to reaction, many other residues also contribute (Bash et al., 1991). These results are consistent with the view that the positive charge at residue 12 counteracts the negative charge of Glu-165 (and possibly Glu-97) and thus enables the anionic substrate to bind. Upon substrate binding, the closed loop conformation of the enzyme stabilizes the reaction intermediate and the enolate-like transition states by ionic interaction with Lys-12 and hydrogen bonding with His-95.

Inorganic phosphate binds to wild-type chicken muscle TIM and induces closure of the loop, while bound sulfate does not result in loop closure (Petsko, 1973). Dihydroxyacetone sulfate (DHAS), which bears only one charge, does not bind and is not a substrate for the wild-type enzyme (Belasco et al., 1978). It would be interesting to see whether the K12M mutant, with the positively charged Lys removed from the active site, could bind DHAS. We predict that it would not, since DHAS is still a monoanion and our electrostatic potential calculations indicate that the mutant active-site potential is net negative. Possibly, a cationic substrate like an amine derivative would be able to bind, but isomerization would probably still not occur. The transition state that must be stabilized has substantial negative charge delocalization on the substrate oxygens, and the net positive potential in the active site of the wild-type enzyme is likely to play a major role in catalysis.

The effect of the K12M substitution on substrate binding, caused by the loss of a single positive charge, is very similar to the effect of introducing a negative charge on substrate binding in isocitrate dehydrogenase when the enzyme is phosphorylated (Dean et al., 1990). In this case, the introduction of a negative charge prevents isocitrate binding to the phosphorylated enzyme, and electrostatic calculations based on the crystal structure data show that the potential in the active site is now negative. It seems likely that a change in charge may be a control mechanism in many enzymes and that simple electrostatic interaction may be a significant element in the overall catalytic act.

ACKNOWLEDGMENT

We thank Jeremy Knowles for counsel and careful reading of the manuscript. We also thank Emil Pai and Nikolaus Schiering for assistance with data collection, Jeff Madura for helpful discussions involving the use of the program UHBD, and Martin Karplus for advice and computer time.

REFERENCES

Alber, T., Banner, D. W., Bloomer, A. C., Petsko, G. A., Phillips, D. C., Rivers, P. S., & Wilson, I. A. (1981) On the three-dimensional structure and catalytic mechanism of triosephosphate isomerase. *Philos. Trans. R. Soc. London B 293*, 159–171.

Alber, T., Davenport, R. C., Jr., Giammona, D. A., Lolis, E., Petsko, G. A., & Ringe, D. (1987) Crystallography and site-directed mutagenesis of yeast triosephosphate isomerase: What can we learn about catalysis from a "simple" enzyme? *Cold Spring Harbor Symp. Quant. Biol. LII*, 603–613.

Albery, W. J., & Knowles, J. R. (1976) Free-energy profile for the reaction catalyzed by triosephosphate isomerase. *Biochemistry 15*, 5627–5631.

Banner, D. W., Bloomer, A. C., Petsko, G. A., Phillips, D. C., Pogson, C. I., & Wilson, I. A. (1975) Structure of chicken triosephosphate isomerase determined crystallographically at 2.5 Å resolution. *Nature (London) 255*, 609–614.

Bash, P. A., Field, M. J., Davenport, R. C., Petsko, G. A., Ringe, D., & Karplus, M. (1991) Computer simulation and analysis of the reaction pathway of triosephosphate isomerase. *Biochemistry 30*, 5826–5832.

Belasco, J. G., & Knowles, J. R. (1980) Direct observation of substrate distortion by triosephosphate isomerase using Fourier transform infrared spectroscopy. *Biochemistry 19*, 472–477.

Belasco, J. G., Herlihy, J. M., & Knowles, J. R. (1978) Critical ionization states in the reaction catalyzed by triosephosphate isomerase. *Biochemistry 17*, 2971–2978.

Blacklow, S. C., & Knowles, J. R. (1990) How can a catalytic lesion be offset? The energetics of two pseudorevertant triosephosphate isomerases. *Biochemistry 29*, 4099–4108.

Blacklow, S. C., Raines, R. T., Lim, W. A., Zamore, P. D., & Knowles, J. R. (1988) Triosephosphate isomerase catalysis is diffusion controlled. *Biochemistry 27*, 1158–1167.

Brünger, A. T., Kuriyan, J., & Karplus, M. (1987) Crystallographic R-factor refinement by molecular dynamics. *Science 235*, 458–460.

Collins, K. D. (1974) An activated intermediate analog. *J. Biol. Chem. 249*, 136–142.

Davenport, R. C., Bash, P. A., Seaton, B. A., Karplus, M., Petsko, G. A., & Ringe, D. (1991) Structure of the triosephosphate isomerase–phosphoglycolohydroxamate complex: An analogue of the intermediate on the reaction pathway. *Biochemistry 30*, 5821–5826.

Davis, M. E., Madura, J. D., Luty, B. A., & McCammon, J. A. (1990) Electrostatics and diffusion of molecules in solution: Simulations with the University of Houston brownian dynamics program. *Comput. Phys. Commun. 62*, 187–197.

Davis, M. E., Madura, J. D., Sines, J., Luty, B. A., Allison, S. A., & McCammon, J. A. (1991) Diffusion-controlled enzymatic reactions. *Methods Enzymol. 202*, 473–497.

Dean, A. M., & Koshland, D. E., Jr. (1990) Electrostatic and steric contributions to regulation at the active site of isocitrate dehydrogenase. *Science 249*, 1044–1046.

Hurley, J. H., Dean, A. M., Thorsness, P. E., Koshland, D. E., & Stroud, R. M. (1990) Regulation of isocitrate dehydrogenase by phosphorylation involves no long-range conformational change in the free energy. *J. Biol. Chem. 265*, 3599–3602.

Joseph, D., Petsko, G. A., & Karplus, M. (1990) Anatomy of a conformational change: Hinged "lid" motion of the triosephosphate isomerase loop. *Science 249*, 1425–1428.

Joseph-McCarthy, D., Rost, L. E., Komives, E. A., & Petsko, G. A. (1994) Crystal structure of the mutant yeast triosephosphate isomerase in which the catalytic base Glutamic Acid 165 is changed to Aspartic Acid. *Biochemistry* (following article in this issue).

Kabsch, W. (1988) Evaluation of single-crystal x-ray diffraction data from a position-sensitive detector. *J. Appl. Crystallogr. 21*, 916–924.

Knowles, J. R. (1991) Enzyme catalysis: Not different, just better. *Nature 350*, 121–124.

Knowles, J. R., & Albery, W. J. (1977) Perfection in enzyme catalysis: The energetics of triosephosphate isomerase. *Acc. Chem. Res. 10*, 105–111.

Komives, E. A., Chang, L. C., Lolis, E., Tilton, R. F., Petsko, G. A., & Knowles, J. R. (1991) Electrophilic catalysis in triosephosphate isomerase: The role of histidine 95. *Biochemistry 30*, 3011–3019.

Kraulis, P. J. (1991) MOLSCRIPT: A program to produce both detailed and schematic plots of protein structures. *J. Appl. Crystallogr. 24*, 946–950.

Laemmli, U. K. (1970) Cleavage of structural proteins during the assembly of the head of bacteriophage T4. *Nature 227*, 680–685.

Lodi, P. J., Chang, L. C., Knowles, J. R., & Komives, E. A. (1994) Triosephosphate isomerase requires a positively charged active site: The role of Lysine-12. *Biochemistry* (preceding article in this issue).

Lolis, E., Alber, T., Davenport, R. C., Rose, D., Hartman, F. C., & Petsko, G. A. (1990) Structure of yeast triosephosphate isomerase at 1.9 Å resolution. *Biochemistry 29*, 6609–6618.

Miller, J. H. (1972) *Experiments in Molecular Genetics*, Cold Spring Harbor Laboratory Press, Cold Spring Harbor, NY.

Nakamaye, K., & Eckstein, F. (1986) Inhibition of restriction endonuclease Nci I cleavage by phosphothioate groups and its application to oligonucleotide-directed mutagenesis. *Nucleic Acids Res. 14*, 9679–9698.

Nickbarg, E. B., Davenport, R. C., Petsko, G. A., & Knowles, J. R. (1988) Triosephosphate isomerase: Removal of a putatively electrophilic histidine residue results in a subtle change in catalytic mechanism. *Biochemistry 27*, 5948–5960.

Petsko, G. A. (1973) D.Phil. Thesis, Oxford University, Oxford, England.

Phillips, D. C., Sternberg, M. J. E., Thornton, J. M., & Wilson, I. A. (1977) An analysis of the three-dimensional structure of chicken triosephosphate isomerase. *Biochem. Soc. Trans. 5*, 642–647.

Pompliano, D. L., Peyman, A., & Knowles, J. R. (1990) Stabilization of a reaction intermediate as a catalytic device: Definition of the functional role of the flexible loop in triosephosphate isomerase. *Biochemistry 29*, 3186–3194.

Raines, R. T., Straus, D. R., Gilbert, W., & Knowles, J. R. (1986) The kinetic consequences of altering the catalytic residues of triosephosphate isomerase. *Philos. Trans. R. Soc. London A 317*, 371–380.

Straus, D., & Gilbert, W. (1985) Chicken triosephosphate isomerase complements an *Escherichia coli* deficiency. *Proc. Natl. Acad. Sci. U.S.A. 82*, 2014–2018.

Straus, D., Raines, R. T., Kawashima, E., Knowles, J. R., & Gilbert, W. (1985) Active site of triosephosphate isomerase: In vitro mutagenesis and characterization of an altered enzyme. *Proc. Natl. Acad. Sci. U.S.A. 82*, 2272–2276.

Wierenga, R. K., Kalk, K. H., & Hol, W. G. J. (1987) Structure determination of the glycosomal triosephosphate isomerase from *Trypanosoma brucei* at 2.4 Å resolution. *J. Mol. Biol. 178*, 487–490.

Wierenga, R. K., Noble, M. E. M., Postma, J. P. M., Groendijk, H., Kalk, K. H., Hol, W. G. J., & Opperdoes, F. R. (1991a) The crystal structure of the "open" and the "closed" conformation of the flexible loop of trypanosomal triose-phosphate isomerase. *Proteins 10*, 33–49.

Wierenga, R. K., Noble, M. E. M., Vriend, G., Nauche, S., & Hol, W. G. J. (1991b) Refined 1.83 Å structure of trypanosomal triosephosphate isomerase crystallized in the presence of 2.4 M ammonium sulfate: A comparison with the structure of the trypanosomal triosephosphate isomerase-glycerol-3-phosphate complex. *J. Mol. Biol. 220*, 995–1015.